JOURNAL OF GEOPHYSICAL RESEARCH, VOL. 112, C07028, doi:10.1029/2006JC003784, 2007

Sediment pumping by tidal asymmetry in a partially mixed estuary

Malcolm E. Scully[1] and Carl T. Friedrichs[2]

Received 28 June 2006; revised 22 February 2007; accepted 11 April 2007; published 28 July 2007.

[1] Observations collected at two laterally adjacent locations are used to examine the processes driving sediment transport in the partially mixed York River Estuary. Estimates of sediment flux are decomposed into advective and pumping components, to evaluate the importance of tidal asymmetries in turbulent mixing. At the instrumented location in the estuarine channel, a strong asymmetry in internal mixing due to tidal straining is documented, with higher values of eddy viscosity occurring during the less-stratified flood tide. As a result of this asymmetry, more sediment is resuspended during the flood phase of the tide resulting in up-estuary pumping of sediment despite a net down-estuary advective flux. At the instrumented location on the adjacent shoal, where no pronounced tidal asymmetry in internal mixing was found, both the pumping flux and advective flux were directed down-estuary. The down-estuary pumping of sediment on the shoal appears to be driven by asymmetries in bed stress. The impact of tidal asymmetries in bed stress at the channel location was negated because the amount of sediment available for resuspension was limited. As a result, the pumping flux was dominated by the overlying asymmetries in internal mixing. The asymmetries in stratification appear to exert an important control on the vertical distribution of sediment by both impacting the eddy diffusivity as well as the fall velocity. During the more turbulent flood tide, the fall velocities are smaller suggesting the Kolmogorov microscale is setting the upper bound on floc diameter.

Citation: Scully, M. E., and C. T. Friedrichs (2007), Sediment pumping by tidal asymmetry in a partially mixed estuary *J. Geophys. Res.*, *112*, C07028, doi:10.1029/2006JC003784.

1. Introduction

[2] Classically, estuarine sediment transport is thought to be driven by the seaward-directed flux of the mean river discharge and landward-directed flux that results from the baroclinic residual circulation [e.g., *Schubel*, 1968]. It is the convergence of these two processes that is most often invoked when explaining the region of elevated turbidity known as the estuarine turbidity maximum (ETM). While the ETM often is located at the upstream limit of the salt intrusion, secondary ETMs are found in the lower reaches of many estuaries [*Lin and Kuo*, 2001]. Although it is likely that this simple convergent process plays a role in maintaining estuarine turbidity in many systems, a number of other processes exert important controls on estuarine sediment transport. The along-channel density gradient that drives the residual baroclinic circulation also creates vertical density stratification, which significantly impacts the turbulent mixing responsible maintaining sediment in suspension [*Scully and Friedrichs*, 2003]. *Geyer* [1993] showed that the suppression of turbulence by stratification plays an important role in trapping sediment in the ETM.

[3] In many partially mixed estuaries, vertically sheared tidal currents interact with the along-estuary salinity gradient, leading to predictable semidiurnal variations in thermohaline stratification [*Simpson et al.*, 1990]. This process, known as tidal straining, promotes vertical mixing during the flood tide and suppresses mixing during the ebb [*Stacey et al.*, 1999; *Geyer et al.*, 2000; *Rippeth et al.*, 2001]. Tidal asymmetries in mixing caused by semidiurnal variations in stratification have been shown to contribute to the landward flux of sediment and contribute to particle trapping within estuaries [*Jay and Musiak*, 1994]. *Scully and Friedrichs* [2003] demonstrated that this mechanism led to a net up-estuary sediment flux even during periods when the residual circulation was directed in the opposite direction. Their results suggested that the asymmetries in stratification did not impact the bed stress, but altered the eddy diffusivity, leading to greater sediment resuspension during the flood tide.

[4] The fall velocity of suspended sediment also exerts an important control on its vertical distribution. In estuarine systems characterized by fine cohesive sediments, particles in suspension often exist in an aggregated state [*Postma*, 1967]. These larger "flocs" typically have higher settling velocities than their component grains. Because this process increases the settling velocity, leading to greater suspension lower in the water column, it increases the trapping effect of

[1] Applied Ocean Physics and Engineering, Woods Hole Oceanographic Institution, Woods Hole, Massachusetts, USA.

[2] Virginia Institute of Marine Science, College of William and Mary, Gloucester Point, Virginia, USA.

0148-0227/07/2006JC003784$09.00

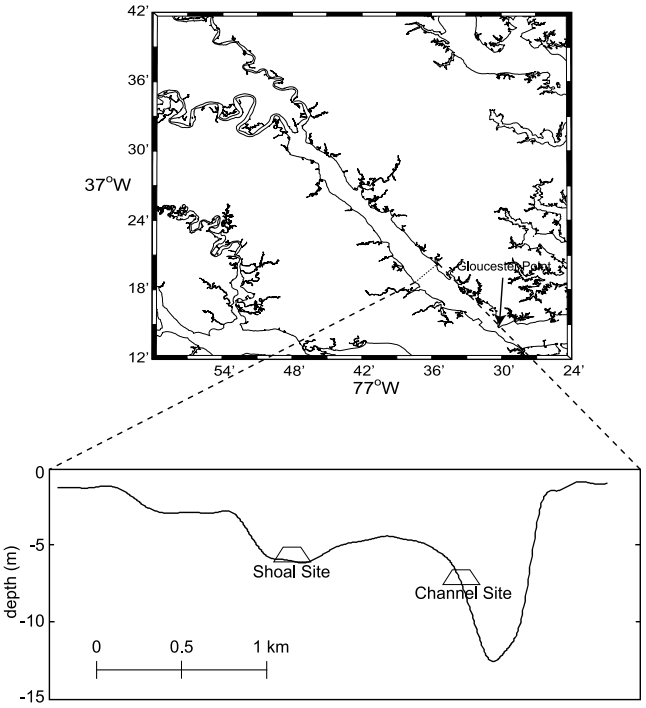

Figure 1. Map of study area, York River Estuary, Virginia with estuarine cross section at "channel" and "shoal" deployment location.

estuarine circulation and augments the formation of the ETM [*Kranck*, 1981]. Aggregates form when individual particles collide owing to Brownian motion, turbulent mixing, or differential settling. Turbulent mixing also is thought to play a role in the break-up of flocs when the length scale of the smallest turbulent eddies and the floc diameter are roughly of the same order [*van Leussen*, 1988]. In the Hudson estuary, *Traykovski et al.* [2004] documented that the floc diameter was inhibited during the energetic portions of the tidal cycle, followed by relatively rapid flocculation when energy decreased. While a number of authors have documented the important relationship between turbulence and settling velocity, its role in estuarine sediment transport has not been fully addressed. It is possible that tidal asymmetries in mixing, which are often observed in estuaries, could result in asymmetries in resuspension that are the result of tidal changes in fall velocity.

[5] This paper is intended to examine the processes driving sediment transport in the York River estuary. It will highlight the importance that tidal asymmetries in turbulent mixing have on sediment resuspension by impacting both the eddy diffusivity as well as aggregation dynamics. In addition to these hydrodynamic effects, the erodibility of sediment in the bed also will be examined. The observational and analytical methods are described in section 2 and the results are presented in section 3. The results are discussed in section 4 and conclusions are presented in section 5.

2. Methods

2.1. Hydrographic Measurements

[6] During the winter of 2003–2004, instrumentation was maintained at two laterally adjacent locations in the estuarine cross-section of the York River near Clay Bank, located roughly 13 km up-estuary from Gloucester Point (Figure 1). At this location in the York River, the main channel of the estuary is located on the northeastern side of the river with a maximum depth of approximately 10 m. A broad shoal extends to the southwest of the main navigational channel with a maximum depth of approximately 6.5 m. Instruments were deployed along the southwestern side of the main channel at a water depth of approximately 7 m ("channel" site) to avoid interfering with navigation, and at the deepest location within the southwestern shoals at a water depth of roughly 6 m ("shoal" site). Although these two locations have similar depths, for the purposes of this paper we assume that they are broadly representative of the deeper channel and shallower shoal regions found in the cross-section. However, because the instruments did not resolve the deepest portion of the channel, the results need to be interpreted with care.

[7] During the experiment, detailed velocity measurements were collected by 4 Sontek acoustic Doppler velocimeters (ADVs), an RDI 1200 kHz acoustic Doppler current profiler (ADCP), and a Sontek 1500 kHz acoustic Doppler profiler (ADP). The 4 ADVs were mounted on a benthic boundary layer tripod deployed at the channel site to provide high-resolution velocity measurements at discrete elevations over the lowest 1.2 m of the water column. The ADVs were mounted 0.10, 0.43, 0.76, and 1.1 m above the bed (mab), on an arm of the tripod that was oriented perpendicular to the along-channel axis of the York River. Unfortunately, the ADVs at 0.43 and 0.76 mab did not function properly and will not be discussed. The ADVs collected three-dimensional velocity measurements in 5-min bursts once an hour at a sampling frequency of 5 Hz. The ADVs were equipped with an acoustic altimetry feature that reported the distance from the sensor to the bed at the end of each burst. The 1200 kHz ADCP was deployed immediately adjacent to the tripod at the channel site and collected vertical profiles of current velocity in 0.50 m bins. The ADCP sampled at roughly 1 Hz and collected one 10-minute burst every hour. The 1500 kHz ADP was deployed at the shoal site and sampled at a rate of 1 Hz averaged over one minute bursts to provide vertical profiles of current velocity in 0.25 m bins.

[8] Three YSI 6000 conductivity, temperature and depth sensors (CTDs) outfitted with optical transmissometers were mounted on the tripod at the channel site at 0.10, 0.41, and 1.5 mab and collected pressure, salinity, temperature, and light transmission every 30 minutes. A mooring that consisted of a YSI 6000 CTD and an InterOcean S4 current meter, outfitted with a CTD was located immediately adjacent to the tripod at the channel site. The CTD and S4 on the mooring were located 2.8 and 3.4 mab, respectively. At the shoal site, two YSI 6600 CTDs located 0.10 and 1.5 mab and an InterOcean S4 sensor with a CTD located 3.5 mab were deployed immediately adjacent to the ADP. As with the YSI 6000, each of the YSI 6600 CTDs was outfitted with a optical transmissometer.

2.2. Suspended Sediment Measurements

[9] All of the CTDs deployed at both the channel and shoals sites were outfitted with optical transmissometers to measure the attenuation of light due to the presence of

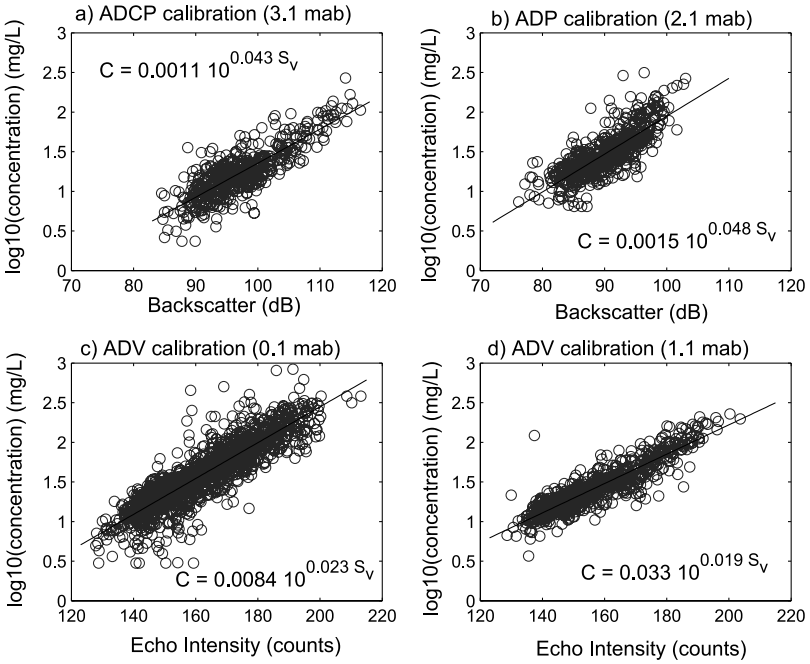

Figure 2. Sediment calibration curves for acoustic backscatter from (a) ADCP (channel), (b) ADP (shoal), (c) ADV 0.1 mab (channel), and (d) ADV 1.1 mab (channel). All calibration curves are plotted against concentration values obtained from co-located transmissometers, except the ADV 1.1 mab, which was calibrated against concentration values obtained from the ADCP.

suspended sediments. Prior to deployment, a two point linear calibration was performed for each transmissometer using deionized water and a fixed laboratory standard of a known value of nephelometric turbidity units (NTUs). While this precalibration ensures that the instruments respond consistently to known values of laboratory standards, in order to convert NTUs to actual concentration values, additional field calibration was necessary. Upon retrieval of the instruments, bottom sediment samples were collected immediately adjacent to the channel deployment site using a benthic grab. In the laboratory, these sediments were mixed in varying levels for calibration purposes. A known quantity of sediment was added to a calibration chamber, where it was maintained in suspension under constant stirring. Each transmissometer was placed in the calibration chamber for roughly one minute to record optical transmission. For each concentration level, water samples were collected and filtered to obtain the mass concentration. A linear calibration between the measured light attenuation and mass concentration was then performed for each instrument in order to obtain estimates of suspended sediment concentration during the experiment.

[10] Each of the transmissometers was equipped with a wiping device that cleaned the optics prior to recording each sample. While the wipers prevented significant biofouling of the instruments, some gradual biofouling was detected during the course of the experiment. In order to remove this effect, a logarithmic curve was fit to the light transmission data during slack water at the beginning and end of the experiment. This logarithmically increasing minimum concentration was then removed by subtracting this curve from the data. This procedure assured the time variation of the minimum concentration observed during slack water by the transmissometer was well correlated with the time variation of the minimum in acoustic backscatter from the ADCP, which was also used to estimate suspended sediment concentration.

[11] Both the RDI ADCP and Sontek ADP record echo intensity (E) at every depth bin. In order to estimate suspended sediment concentration, E which is measured in counts and is proportional to the logarithm of power, must be converted to decibels (dB) by the factor K_c. Following *Deines* [1999] the sonar equation can be represented as

$$S_v = C_o + 20\log 10(R) + 2\alpha R + K_c(E), \qquad (1)$$

where S_v is the acoustic backscatter in dB, C_o is a linear calibration constant that encompasses a number of factors including transmit pulse length, transmit power, and system noise. The loss of acoustic energy due to spherical spreading and the attenuation due to water are represented by the second and third terms on the right hand side of the equation, where R is range along the beam to the scatterers (m) and α is the absorption coefficient of water (dB/m). The coefficient K_c is unique to each instrument, but has a reported range of values of 0.35 to 0.55 dB/Bit [*Deines*, 1999]. In order to estimate K_c for each instrument, we assume that there are periods of vertically uniform scattering during slack water when the vertical differences in E are solely due to the spreading and attenuation terms. Because of possible errors associated with additional attenuation due to suspended sediment [*Thorne and Hanes*, 2002], values of K_c were estimated near the bed where attenuation is minimal. This method resulted in $K_c = 0.52$ for both the ADCP and ADP. Using K_c, E was then converted to dB and range corrected.

[12] Previous work suggests that there is a consistent relationship between the concentration of fine sediment in

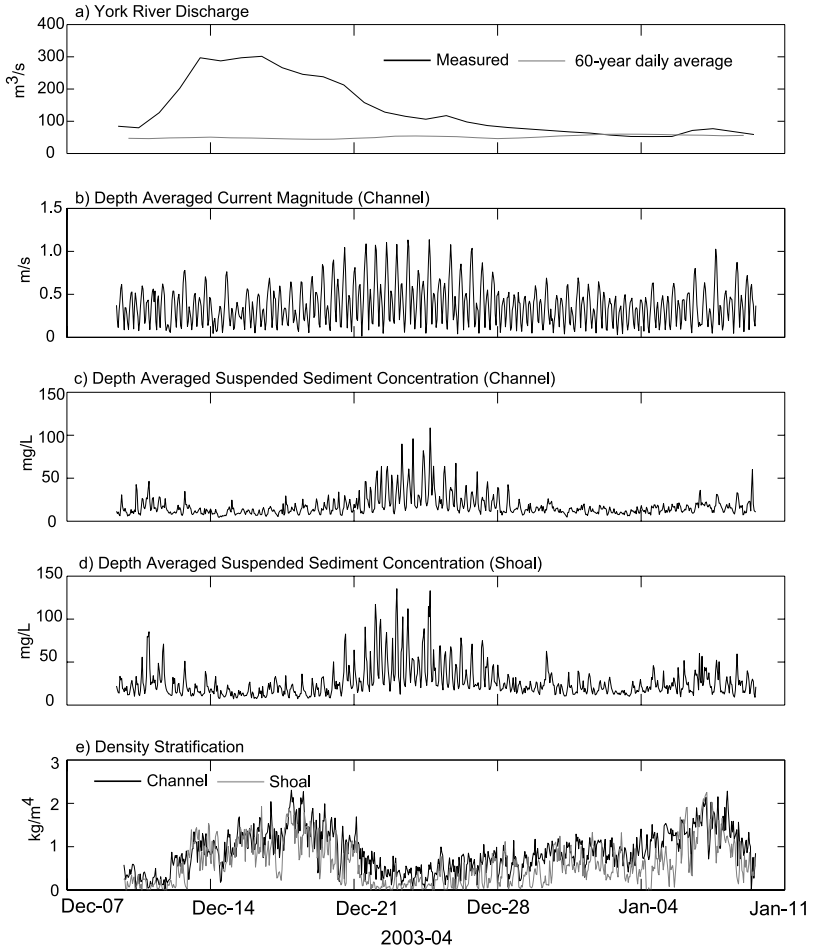

Figure 3. Time series data December 2003 to January 2004: (a) combined daily river discharge from United States Geological Survey's Mattaponi and Pamunkey gauging stations, with 60-year daily average, (b) depth-averaged current magnitude measured by ADCP at the channel site, (c) depth-averaged sediment concentration measured by calibrated ADCP backscatter at the channel site, (d) depth-averaged sediment concentration measured by calibrated ADP backscatter at the shoal site, and (e) density stratification measured between the highest and lowest CTDs at the channel site (dark line) and the shoal site (light line).

estuaries (C in mass per volume) and the acoustic backscatter of the form [*Holdaway et al.*, 1999; *Fugate and Friedrichs*, 2002],

$$C = A\,10^{\beta Sv}, \tag{2}$$

where A and β are calibration coefficients. Figure 2a shows the best fit least squares regression between the concentration estimate from the transmissometer at the channel location deployed 3.1 mab and the acoustic backscatter measured by the ADCP at the vertically adjacent bin. Figure 2b shows the same relationship for the shoal site, between the transmissometer 2.1 mab and the acoustic backscatter measured by the ADP at the vertically adjacent bin. For both the ADCP and ADP data there is a relatively high correlation between the acoustic backscatter and the log10 of the concentration as estimated by the adjacent transmissometer (r = 0.82 and 0.80, respectively).

[13] Just as the backscatter from the ADCP and ADP can be calibrated, so can the echo intensity of the ADVs. In fact, because no range correction is necessary to adjust the point measurement of the ADV, the procedure is relatively simple. On the main channel tripod, the lowest ADV and transmissometer were roughly located at the same height above the bed. A simple empirical calibration was performed according to equation (2). A similar calibration was performed for the highest ADV. However, because there was no vertically adjacent transmissometer, the concentration profile obtained from the ADCP had to be interpolated down to the height of the upper ADV. This was done using a second-order polynomial. Because the profiles were only extrapolated over roughly 0.40 m, the estimate was relatively insensitive to the method of extrapolation. Figures 2c and 2d show the best fit least squares regression for the calibration of the ADVs deployed 0.10 and 1.1 mab at the channel site (r = 0.87 and r = 0.90, respectively).

[14] Figure 2 clearly indicates that there is a large amount of scatter in the various estimates of concentration, with a range of the order of ± half a decade in estimates of concentration for the same backscatter level. It is possible that much of this variability is due to changes in particle size as turbulent intensity varies, including potentially system-

atic differences between flood and ebb tides. While both optical and acoustic methods of inferring sediment concentration are sensitive to grain size, recent work has demonstrated that the use of acoustic backscatter is significantly less sensitive than optical methods when particles are composed of loose muddy aggregates. In particular, the results of *Fugate and Friedrichs* [2002] strongly suggest that in estuarine environments, acoustic methods of estimating concentration are relatively insensitive to changes in particle size caused by flocculation of muddy sediment. This is presumably because acoustic backscatter responds to the size of the component grains that cause the acoustic impedance, not the entire aggregate. The presence or absence of flocculated particles does not dramatically change the acoustic impedance because flocculated aggregates are so loosely bound. In contrast, optical methods are less accurate because they respond directly to surface area of the entire floc.

[15] In this study, while optical methods were used to assist in calibrating the acoustic instruments, all estimates of sediment concentration used in the sediment transport calculations were based on calibrated acoustic backscatter. Thus much of the scatter in the calibration curves may be caused by the sensitivities of the optical estimates of concentration to floc size, not from the acoustic response. The actual acoustic estimates of sediment concentration used in the analysis are likely to be more stable than the calibration against optical observations suggest, because of the floc size sensitivity of the optical methods. For these reasons, it is unlikely that the main patterns documented in this manuscript are artifacts of floc size sensitivities in the calibration. The improvement associated with relying on acoustic backscatter can be seen directly in Figure 2d, which is an acoustic-to-acoustic sensor comparison. Figure 2d exhibits less scatter, particularly with respect to outliers, relative to Figures 2a–2c, which are acoustic-to-optical comparisons. Nonetheless, there is still notable scatter in Figure 2d, and limitations in the absolute accuracy of all sediment transport calculations inferred from optical or acoustic backscatter must be kept in mind.

3. Results

[16] The 2003–2004 experiment took place during a period of elevated rainfall. Discharge from the York River tributaries for December 2003 was, on average, nearly 3 times the 60-year average (Figure 3a). The experiment spanned approximately 30 days, covering the full spring-neap tidal cycle. The spring-neap cycle was apparent in the both the depth-averaged current magnitude (Figure 3b), as well as the depth-averaged suspended sediment concentration at both the channel (Figure 3c) and shoal (Figure 3d) locations. With the elevated river discharge, there was persistent vertical density stratification throughout much of the experiment at both the channel and shoal sites, especially during neap tide (Figure 3e). The vertical stratification exceeded 2 kg/m^4 on several occasions at both locations, and median values of stratification measured between the uppermost and lowermost sensors were 0.88 and 0.58 kg/m^4 at the channel and shoal sites, respectively. In addition, significant tidal asymmetries in stratification were observed at both locations. At the channel site, the median stratification on flood and ebb was 0.81 and 0.94 kg/m^4, respectively. The asymmetry had the opposite sense at the shoal site, where the flood was actually more stratified on average than the ebb (0.65 and 0.53 kg/m^4).

[17] With co-located estimates of sediment concentration and current velocity, it is straightforward to estimate sediment flux. Although there is stronger residual outflow over the channel site (Figure 4a), the sediment flux is more strongly seaward directed at the shoal location (Figure 4b). Figure 4b shows the average profiles of sediment flux for the channel and shoal sites, using the ADCP and ADP concentration and velocity data. To examine these patterns in more detail, the sediment flux can be divided into an advective flux and a pumping flux, similar to the methods used by *Geyer et al.* [2001]. The advective flux is driven by the tidally-averaged velocity and tidally-averaged concentration, given as

$$Q_A = \langle U(z)\rangle\langle C(z)\rangle, \tag{3}$$

where U is the along-channel velocity, C is the suspended sediment concentration, and the angled brackets denote tidal averages (tides were removed using a 35-hour low-pass filter). The pumping flux is then given as

$$Q_P = u'(z)\ c'(z), \tag{4}$$

where the primes indicate the deviations from the tidally averaged values. This decomposition of the flux enables us to more closely examine the processes driving sediment flux at the two locations. Figures 4c and 4d show the profiles of the advective and the pumping sediment flux, averaged over the deployment, for both channel and shoal locations, respectively. At the channel location, although the average advective flux is down estuary throughout the water column, the pumping flux is directed up estuary near the bed. In fact, the magnitude of the pumping flux is greater than the advective flux near the bed, resulting in a net up-estuary transport of sediment as measured by the lowest bin of the ADCP. At the shoal location, both the advective and pumping fluxes are directed down-estuary.

[18] The up-estuary sediment pumping observed near the bed at the channel location is driven by tidal asymmetries in sediment resuspension. Figure 4e shows profiles of the median sediment concentration for both the channel and the shoal location, segregated by the phase of the tide. Despite larger velocities on the ebb phase of the tide at the channel location, sediment concentrations are significantly greater during the flood phase of the tide. At the shoal location the pattern is less clear (Figure 4f). Although concentrations appear to be greater on the flood near the bed, they are greater on ebb higher in the water column. At the shoal location, where the flood tide was slightly more stratified on average than the ebb, the net sediment pumping is ebb directed. *Scully and Friedrichs* [2007] used the dominant terms in the axial momentum balance to estimate vertical profiles of eddy viscosity for both the channel and shoals locations. Figure 5 shows the profiles of eddy viscosity calculated by *Scully and Friedrichs* [2007], segregated by the phase of the tide, as well as for spring and neap tidal conditions. At the channel location, there is a clear tidal asymmetry in eddy viscosity, with larger values reported for the flood tide. This asymmetry is particularly pronounced during spring tidal conditions and exists despite

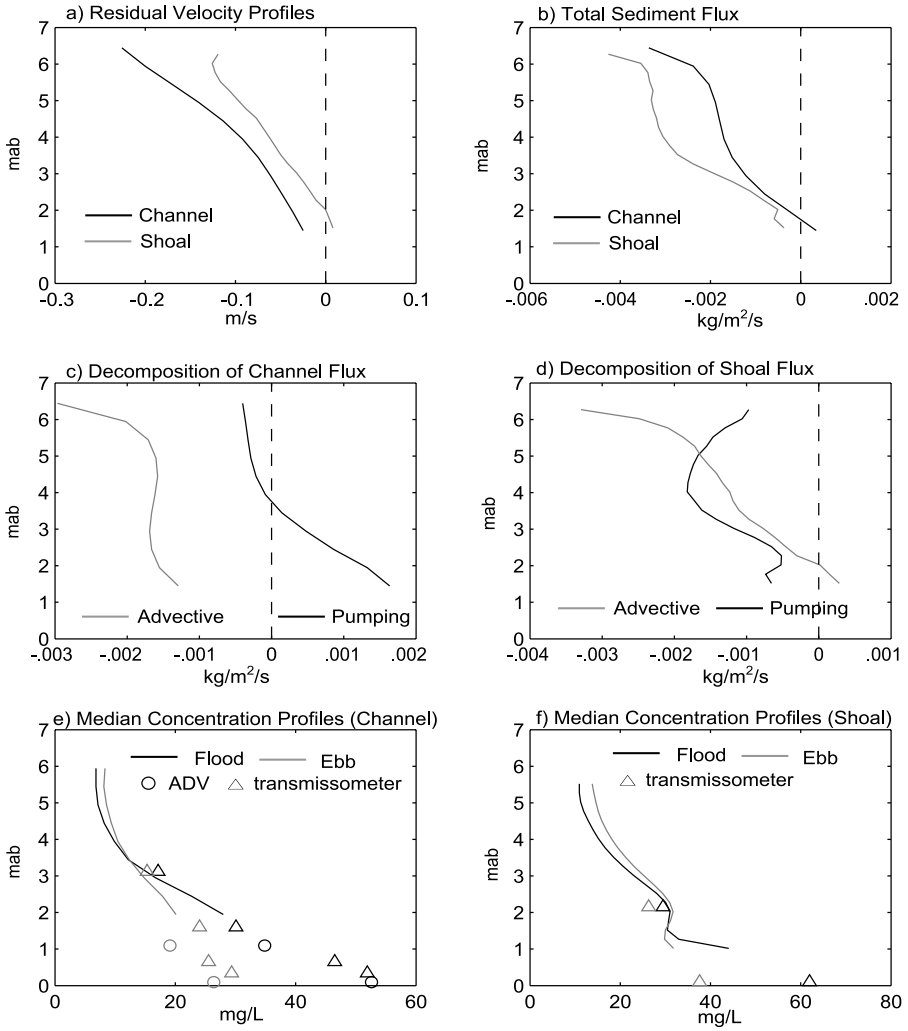

Figure 4. (a) Depth-averaged along-channel velocity profiles measured by ADCP at the channel site (dark line) and ADP at the shoal site (light line), (b) depth-averaged along-channel sediment flux profiles measured by ADCP at the channel site (dark line) and ADP at the shoal site (light line), (c) depth averaged profiles of sediment pumping flux (dark line) and advective flux (light line) at the channel site, (d) depth averaged profiles of sediment pumping flux (dark line) and advective flux (light line) at the shoal site, and (e) tidally averaged sediment concentration profiles for flood (dark line and symbols) and ebb (light line and symbol) at the channel site obtained from calibrated ADCP (lines). Circles represent values obtained from calibrated ADV backscatter and triangles represent values from calibrated transmissometers. (f) Tidally averaged sediment concentration profiles for flood (dark line and symbols) and ebb (light line and symbol) at the shoal site obtained from calibrated ADP (lines). Triangles represent values from calibrated transmissometers.

the fact that strong down estuary residual flows are reported during this period. At the shoal location, there is no pronounced asymmetry in the eddy viscosity profiles, and the suspended sediment profiles do not exhibit the strong tidal asymmetry observed in the channel.

[19] The impact that the tidal asymmetry in eddy viscosity has on sediment pumping is clearly evident when examining the time series of sediment pumping in Figure 6. Figure 6 shows the time series of the depth integrated total flux, advective flux and pumping flux at both the channel and shoal sites. As expected, the magnitude of total sediment flux is greatest at both locations during the spring tide. Despite the similarity in the overall magnitude of sediment flux at the two locations, the patterns of advective and pumping fluxes are significantly different. During the spring tides the advective flux and pumping flux measured at the channel site often are in the opposite direction, while both components of sediment flux measured at the shoal location are directed down-estuary. At the channel location, the strong down-estuary advective flux is offset and even at times reversed by the up-estuary sediment pumping. The opposite sense of the advective and pumping sediment fluxes at the channel location is largely a consequence of tidal asymmetries in stratification. During the ebb tide at the channel location, the increased stratification damps turbulent mixing, limiting sediment resuspension. The preferential damping of turbulence during the ebb tide at the channel location enhances up-estuary sediment pumping. This effect

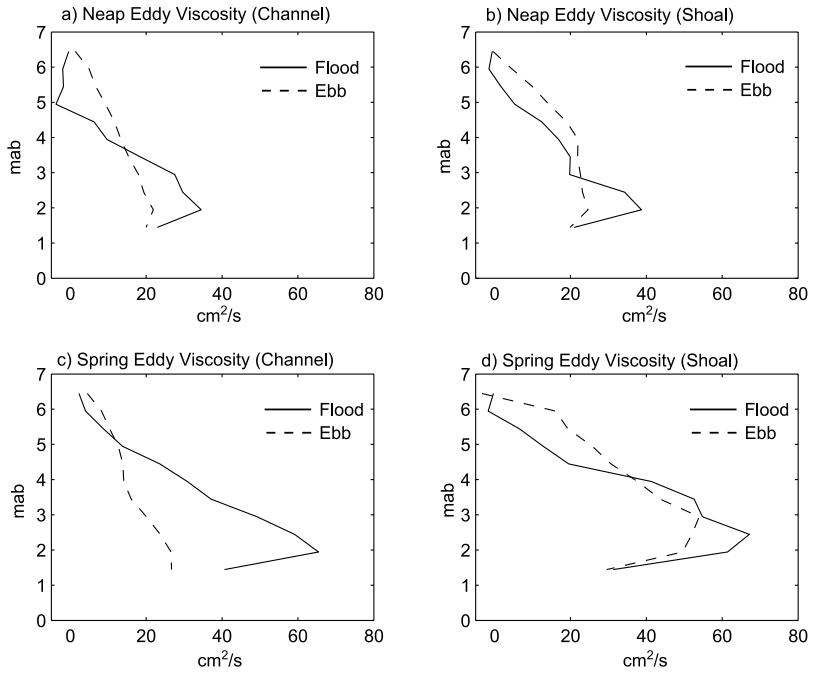

Figure 5. Median profiles of the eddy viscosity from *Scully and Friedrichs* [2007] estimated from the momentum integral for both channel and shoal sites during spring and neap tidal conditions (solid line denotes flood and dashed line denotes ebb).

may be accentuated because the tripod at this location is located on the flank of the channel, not in the deepest part of the cross section. As a result, the boundary may be more strongly stratified than in the deeper portions of the channel.

4. Discussion

4.1. Influence of Sediment Availability

[20] Tidally asymmetries in sediment resuspension may be simply manifestations of tidally asymmetries in bed stress, driven by the residual mean circulation. Such an asymmetry would contribute to the pumping flux and would be positively correlated with the mean flux. However, this contribution to the pumping flux could be negated if the amount of sediment available for resuspension in the bed is limited. Under supply-limited conditions, tidal asymmetries in bed stress may not lead to commensurate asymmetries in resuspension. During the spring tide the ADV data at the channel site suggests that the residual stress is ebb-directed

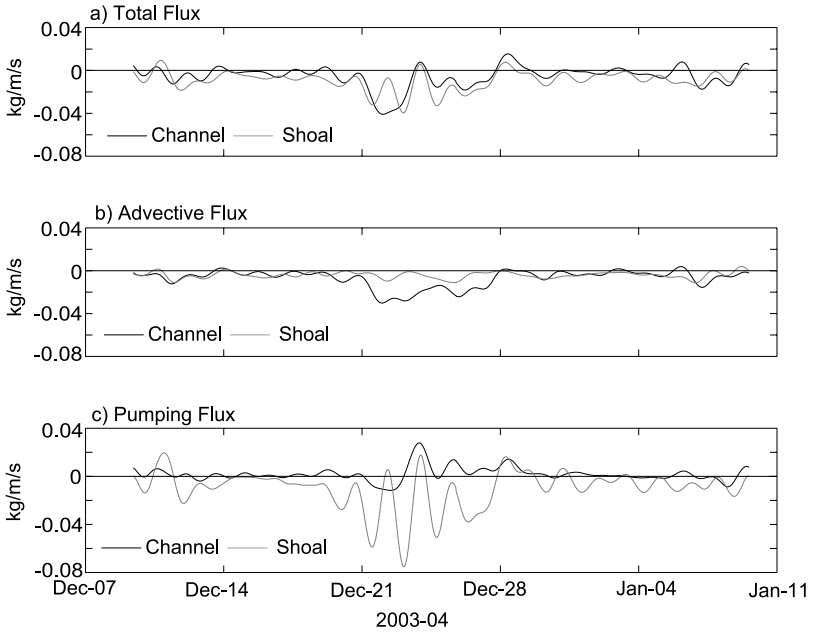

Figure 6. Time series of depth-integrated (a) total sediment flux, (b) advective sediment flux, and (c) pumping sediment flux (dark lines represent the channel site and light lines represent the shoal site).

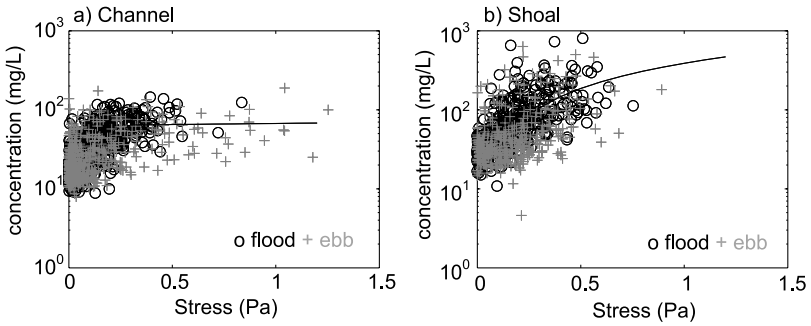

Figure 7. Bed stress versus concentration measured 0.10 mab for (a) channel site and (b) shoal site. Circles indicate flood and crosses indicate ebb. Stress at the channel site was measured by the ADV 0.12 mab and stress at the shoal site was estimated using a drag coefficient (0.0023) and quadratic velocity measured 1.0 mab. Lines indicate a linear regression fit to all data where the stress exceeded 0.3 Pa.

[*Scully and Friedrichs*, 2007]. In the absence of supply limitation, this asymmetry in stress should increase the resuspension on ebb and help offset the sediment pumping due to the overlying internal asymmetry. However, there is a strong divergence between the advective and pumping fluxes at the channel site during the spring tide, suggesting that the increased stress on ebb is not driving asymmetries in resuspension that are leading to down-estuary pumping. In contrast, at the shoal location the asymmetry in bed stress does appear to contribute to greater resuspension during the ebb and both the advective and pumping fluxes are directed down-estuary during the spring tide.

[21] The ADV data that were collected 0.12 mab at the channel site are used to further investigate the role that sediment erodibility plays in the observed patterns of sediment flux. This data provides both a direct measure of the bed stress, as well as an estimate of the concentration very close to the bed. Although *Scully and Friedrichs* [2007] demonstrated that stratification can impact the relationship between stress and velocity, even over the lower meter of the water column, we assume that the stress and concentration data 0.12 mab are relatively unaffected by the overlying stratification. This enables us to more closely examine the relationship between bed stress and a reference concentration independently from any overlying internal asymmetry. Figure 7a shows a plot of the bed stress against the concentration, as measured by the ADV. Flood and ebb data are plotted separately. At lower values of stress, there is clearly a positive relationship between the bed stress and near-bed concentration. However, once a stress of approximately 0.3 Pa is exceeded, there is no clear positive correlation. In fact, a linear regression yields a negative slope when fit to all data above 0.3 Pa. This pattern clearly suggests that the resuspension of sediment, particularly under higher-stress conditions, is supply limited. Because the residual stress tended to be ebb directed during high-stress conditions, supply limitation prevents a significant asymmetry in resuspension that would favor down-estuary sediment pumping.

[22] Unfortunately, no direct estimates of stress were available at the shoal location. However, we can estimate stress using a quadratic drag relationship and examine the potential for supply limitation the shoal location. Figure 7b plots the quadratic stress estimated using the ADP velocity measured approximately 1 mab and the drag coefficient estimated by *Scully and Friedrichs* [2007], against the concentration estimate from the lowest transmissometer (0.10 mab). In contrast to the results shown in Figure 7a, at the shoal location there is a consistent increase in near-bed concentration with increasing stress, even at the higher levels of stress. It should be noted, that the drag coefficient used to estimate stress is sensitive to changes in stratification, so these results should be interpreted with caution. However, it does not appear that supply limitation is significantly impacting the shoal location, providing an explanation for why the pumping and advective terms are in the same direction at this site.

[23] The patterns of sediment flux observed appear to be influenced by long-term changes in bed erodibility. A relatively simple way of evaluating erodibility is to assume that the sediment concentration (C_a) near the bed is related to the bed stress (τ_b), multiplied by some constant (γ),

$$C_a \propto \gamma \tau_b. \tag{5}$$

This is a simplification of a complex process, but is analogous to the reference concentration approach commonly used to model sediment transport [*Smith and McLean*, 1977]. However, because we do not know the critical erosion threshold, which changes with both time and depth into the bed, we lump all of the changes in erodibility into a single coefficient (γ). This provides a simple way of looking at temporal changes in erodibility.

[24] The parameter γ can be estimated from the ADV estimates of stress and concentration measured by the lowest sensor at the channel location. Estimates of γ are noisy because we are often dividing by number that is approaching zero. To try to remove this effect, the bed-stress and concentration were both smoothed using a 96-hour running median. The time series estimate of γ using the smoothed data is shown in Figure 8a. The estimate of γ exhibits significant temporal variability, changing by a factor of 4 over timescales shorter than the spring-neap cycle. The changes in γ are positively correlated with changes in the bed elevation (Figure 8b) as measured by the altimetry feature of the ADV ($r = 0.70$), suggesting that the sediment becomes increasingly more difficult to erode with depth into the bed. During the period from 18 December to 28 December, approximately 2 cm of sediment appear to be removed from the bed. During this period, there is a

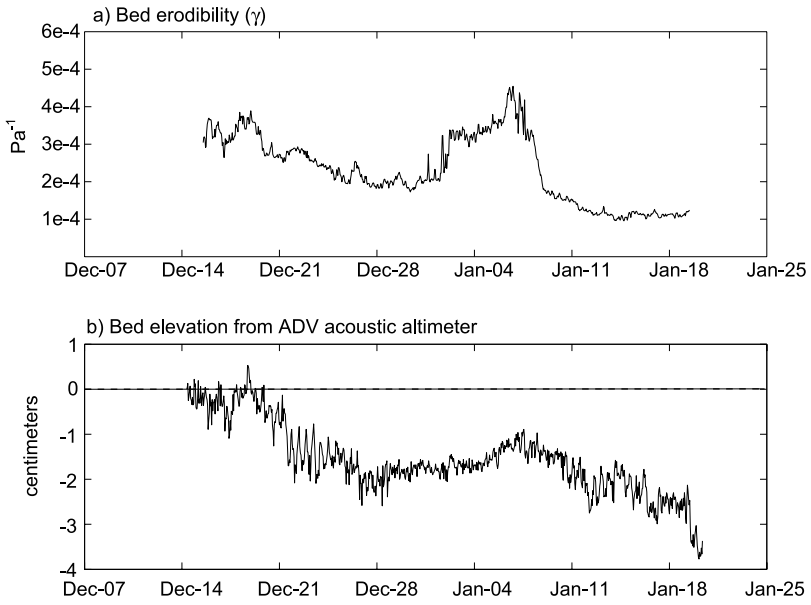

Figure 8. (a) Sediment erodibility estimated at the channel location, using ADV concentration and stress measured 0.10 mab. (b) Bed elevation measured by the acoustic altimetry feature of the ADV 0.10.

steady decease in γ suggesting the underlying sediment is more consolidated and more difficult to remove. Bed elevation increases slightly from 28 December to 7 January, which is accompanied by an increase in the erodibility as parameterized by γ.

[25] The increase in erodibility with depth, leads to a hysteresis effect during spring tidal conditions. During the beginning period of the spring tide, when stress is increasing, the easily eroded sediment is removed from the bed. As a result, less sediment can be eroded for a similar value of stress during the second half of the spring tide, when stress is decreasing. This hysteresis appears to significantly impact the processes governing sediment pumping. During the early portion of the spring tide, when tidal energy is still increasing, supply limitation is not significant, and asymmetries in bed stress can lead to asymmetries in resuspension. The residual stress is ebb directed and this early portion of the spring tide is the only period when significant down-estuary sediment pumping is observed at the channel location. During the second half of the spring tide when the residual stress is still ebb directed, supply limitation negates the impact of the asymmetry in bed stress and sediment pumping is dominated by the overlying internal asymmetry. It is during this period of decreasing stress when the greatest up-estuary sediment pumping occurs. Because the amount of sediment resuspended near the bed is controlled by its availability and not by the magnitude of the bed stress, the stronger bed stress on the ebb tide does not contribute to down-estuary sediment pumping. The up-estuary pumping is driven by the overlying eddy viscosity, which is larger on flood because of tidal straining. This hysteresis effect is not seen at the shoal location, and as a consequence, the sediment pumping term is directed down estuary, consistent with the asymmetry in bed stress. The greater availability of sediment for resuspension at the shoal location is likely the result of across-estuary secondary circulations. Both the modeling results of *Geyer et al.* [1998] and the observational results of *Woodruff et al.* [2001], demonstrate preferential accumulation of sediment on the western shoal of the Hudson River estuary.

4.2. Fall Velocity

[26] The results of *Scully and Friedrichs* [2003] demonstrate that tidal asymmetries in internal mixing lead to sediment pumping by controlling the vertical distribution of sediment in the water column. Changes in the sediment fall velocity also can have a significant impact on the vertical distribution of sediment. In estuaries with fine cohesive sediments, sediment particles often exist in loosely bound aggregates [*Eisma*, 1986]. While the processes that control the aggregation and disaggregation of particles are complex, there is evidence that the level of turbulent shear significantly impacts flocculation dynamics. The results of *Kranck and Milligan* [1992] demonstrate an inverse relationship between the level of turbulence and floc diameter. Thus the internal asymmetry in mixing caused by changes in stratification may impact the vertical distribution of sediment, not only through its impact on the eddy diffusivity, but also by altering the sediment fall velocity.

[27] *Fugate and Friedrichs* [2002] used calibrated ADV backscatter to estimate the fall velocity of aggregated estuarine particles. This method assumes that at first order the concentration of suspended sediment at a given height above the bed can be represented as a balance between the downward settling flux and the upward turbulent diffusive flux,

$$-w_s\langle c\rangle = \langle c'w'\rangle, \tag{6}$$

where w_s is the sediment fall velocity, c is concentration, w is vertical velocity, and the primes denote fluctuations from the mean, which is denoted by the angled brackets. The slope of a linear regression between the turbulent diffusive flux and the concentration as measured by the ADV, gives an estimate of the fall velocity. This method was applied, and Figures 9a and 9b plot the relationship between the estimated turbulent diffusive flux and the concentration

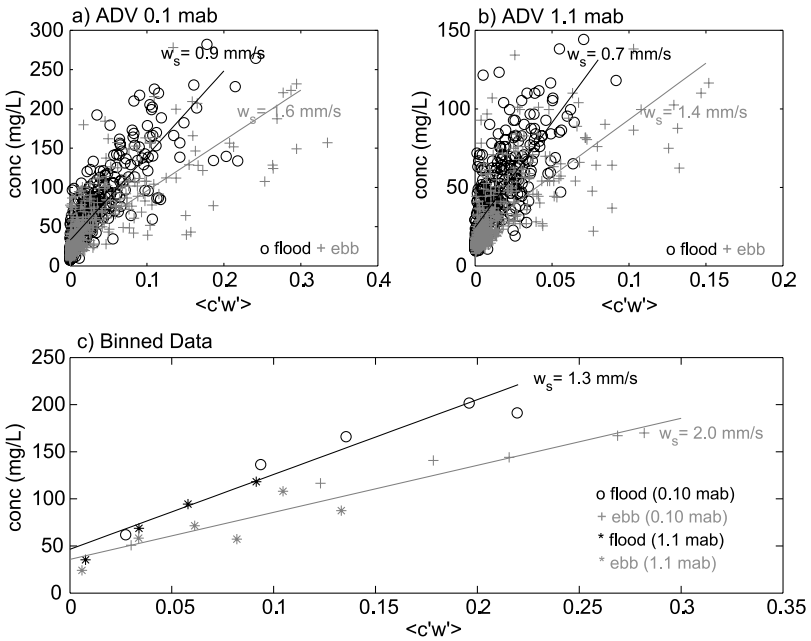

Figure 9. Estimate of fall velocity from ADV data obtained by regressing the turbulent diffusive sediment flux against concentration as measured by the ADVs (a) 0.10 mab, (b) 1.1 mab, and (c) after binning data from each ADV into equal increments based on concentration.

measured by the ADVs 0.12 and 1.06 mab, respectively. Values for flood and ebb are plotted separately. Because the data are somewhat noisy, they were grouped into roughly 6 equally spaced bins based on the concentration, and the median values are plotted in Figure 9c. In Figure 9c, flood and ebb data are plotted using different symbols, as are the data from the two different ADVs. In both the binned and non-binned data, estimates of the fall velocity are higher during ebb than they are during the flood. Estimates from linear regressions fit to the binned data give fall velocity values of 2.0 and 1.3 mm/s for ebb and flood, respectively. These values are significantly higher than would be expected for the disaggregated fine sediment found in the York River, suggesting that much of the sediment is packaged as flocculated aggregates.

[28] Given the evidence for an internal asymmetry in turbulent mixing (Figure 5), it is possible that the inferred tidal asymmetries in the fall velocity could be the result of asymmetries in turbulent mixing caused by the changes in stratification. During the less stratified and more turbulent flood tide, greater break up of the aggregated particles may occur, resulting in a lower settling velocity. Because the nonsettling background concentration changes over meteorological timescales [*Fugate and Friedrichs*, 2002], it is difficult to directly solve equation (6) to examine the temporal behavior of the estimated fall velocity. However the nonintegrated form of the sediment conservation equation can be used if you assume that there are no vertical gradients in the slowly settling background concentration,

$$dc/dt = -w_s dc/dz - d/dz\langle c'w'\rangle. \quad (7)$$

With estimates of concentration and diffusive sediment flux at two heights, equation (7) can be used to estimate the time series of sediment fall velocity, without bias from the background non-settling wash load. This approach allows for a more detailed examination of the impact of turbulence on fall velocity.

[29] Turbulent energy is generated by large-scale turbulent eddies and dissipated by viscosity at very small scales. As the level of turbulence increases, dissipation is driven to smaller and smaller length scales. The length scale of the smallest turbulent eddies is often presented as the Kolmogorov microscale,

$$\eta = \left(\nu^3/\varepsilon\right)^{1/4}, \quad (8)$$

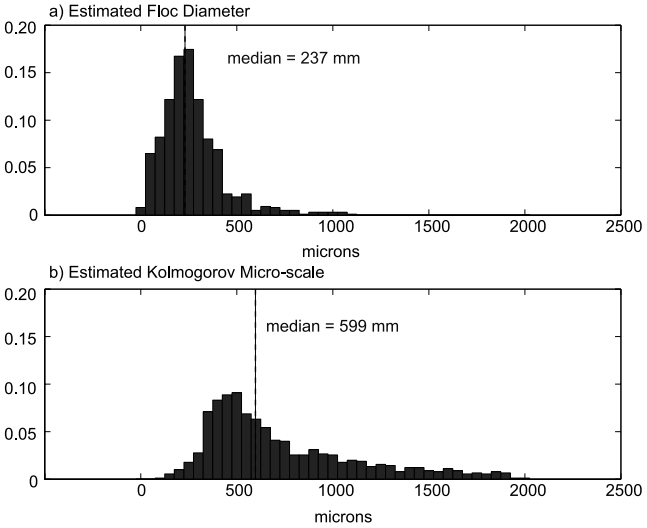

Figure 10. Frequency histogram of (a) floc diameter calculated from the ADV estimate of velocity following equation (10). (b) Kolmogorov microscale, estimated following equation (8).

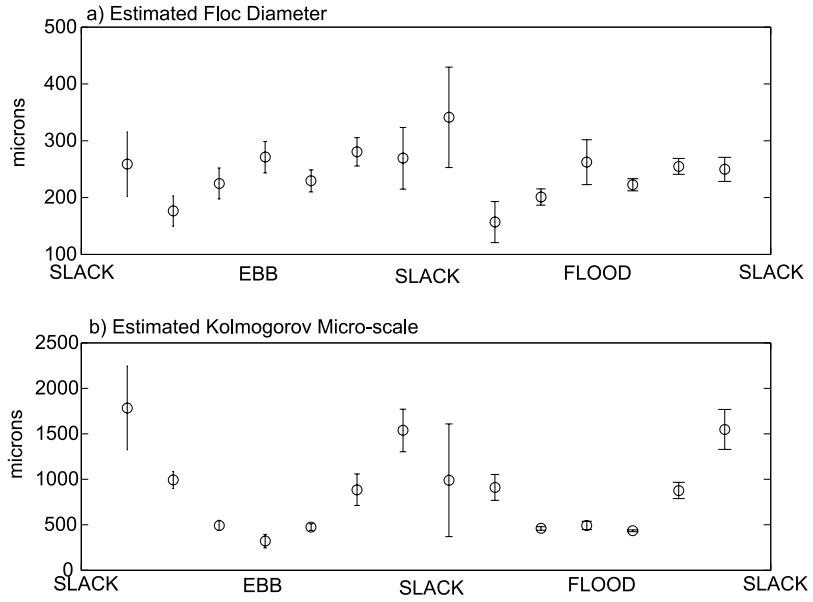

Figure 11. (a) Averaged tidal cycle values of the floc diameter estimated following equation (10) and (b) the Kolmogorov microscale estimated from equation (8). Vertical lines represent 1 standard error.

where ν is the kinematic viscosity of water and ε is rate of turbulent dissipation. A number of authors have suggested that the Kolmogorov microscale sets the upper bounds of the size that flocculated particles can reach before they are sheared apart by turbulence [*van Leussen*, 1988]. Assuming that the production of turbulence must be balanced by dissipation, and applying log layer scaling, turbulent dissipation can be estimated as

$$\varepsilon = u_*^3/\kappa z, \tag{9}$$

where u_* is the turbulent shear velocity, κ is von Karman's constant (0.41) and z is the height above bed. Using the Reynolds stress estimates from ADVs deployed at the channel location to calculate u_*, it is possible to estimate turbulent dissipation. Although there were no direct measurements of the size of the flocs during this experiment, other authors have developed empirical relationships relating fall velocity to aggregate diameter. *Sternberg et al.* [1999] suggested the following relationship between the observed floc diameter (D in microns) and the observed fall velocity (w_s in mm/s) for aggregated particles on the continental shelf of northern California,

$$w_s = 0.0002\, D^{1.54}. \tag{10}$$

Using this relationship, we can estimate the diameter of the flocculated particles from the estimate of fall velocity. Figure 10a shows a frequency histogram of floc diameter based on all of the data calculated following equation (7). Figure 10b shows a similar histogram but for the estimated Kolmogorov microscale estimated following (8). Consistent with the results of *Berhane et al.* [1997] from work on the Amazon shelf, the average floc diameter is roughly half the average value of η.

[30] Despite the fact that the median value of η is larger than the estimated median diameter of the aggregated particles, there is significant overlap between the two histograms. Clearly in an estuary, the level of turbulence will vary at the tidal timescale. During slack conditions, η will be significantly larger than during peak flow. To look at the tidal variability of both η and the estimated floc diameter (D), the data were segregated by the phase of the tide using the velocity time series and the median values were plotted to represent an "average" tidal cycle. Figure 11 compares the average tidal cycle values of D and η. As expected, the values of η vary significantly during the tidal cycle. However, during maximum flood and maximum ebb, the value of η approaches that of D suggesting that under peak flow, the smallest scale of turbulence is approximately the same size as the flocculated particles.

[31] Because the estimated dissipation is based upon simple log layer scaling using the measured bottom stress, which is largely unaffected by the overlying stratification, it is likely that the estimates of η do not realistically represent the impact of the internal asymmetry shown in Figure 5. However, there does appear to be some evidence for the impact of this asymmetry in the tidal estimates of the floc diameter. There is a general trend for floc diameter to increase throughout both flood and ebb tide, reaching maximum values near slack water. The values decrease back to near minimum as the tidal currents begin to accelerate. However, floc growth during the flood is slower than during ebb, indicating greater limitation by the turbulent length scale during flood. It is clear from Figure 11 that the timescale of floc growth is substantially slower than the rate of change of η. Thus, while the maximum floc diameter may be set during energetic conditions, the floc growth rate is too slow for the aggregates to exist in an dynamic equilibrium where floc growth is balanced by floc breakup as suggested by *Jackson* [1995]. It appears that the suspension exists in a partially flocculated state as suggested by *McCave* [1985], where the aggregation rate is slow and settling removes sediment from suspension before complete flocculation can occur. In this situation, a tidal asymmetry in

fall velocity caused by turbulent floc break-up is not only dependent upon the relative asymmetry in the Kolmogorov length scale, but also on the floc growth rate.

5. Conclusions

[32] The net estuarine sediment transport is most often attributed to the landward flux of sediment, driven by the residual baroclinic estuarine circulation. However, tidal asymmetries in sediment resuspension can lead to sediment pumping, which are often the same order of magnitude as the residual advective flux. These asymmetries in resuspension can be driven either by asymmetries in bed stress or by asymmetries in internal mixing. Unlike asymmetries in bed stress, which are driven by the direction of the net pressure gradient forcing, asymmetries in internal mixing are impacted by tidal asymmetries in stratification. As a result, the eddy viscosity can be greater on flood than on ebb, even when the residual stress is ebb directed. Thus asymmetries in bed stress and asymmetries in internal stress can influence tidal asymmetries in sediment resuspension with the opposite sense.

[33] Observations of sediment flux collected from the channel location in the York River appear to be dominated by tidal asymmetries in internal mixing. At this location, tidal straining of the density field leads to greater sediment resuspension during the flood tide, resulting in up-estuary sediment flux even when the advective residual is directed down-estuary. The internal asymmetry dominates at the channel location because supply limitation effectively decouples the asymmetry in bed stress from sediment resuspension. The opposite appears to be the case at the shoal site where the advective and pumping fluxes are both directed down-estuary. Neither supply limitation nor significant tidal asymmetry in internal mixing were observed at the shoal location, leading to down-estuary sediment pumping. Thus, during the energetic spring tidal condition, there was significant up-estuary sediment pumping in the channel with down-estuary pumping over the shoals. Tidal asymmetries in fall velocity may have contributed to the up-estuary sediment pumping at the channel location. Estimates of fall velocity were greater during the more stratified ebb than they were during the flood tide near the bed. This asymmetry may reflect the tidal asymmetry in internal mixing caused by tidal straining. Estimates of the median floc diameter and the Kolmogorov microscale were the same order during periods of peak tidal flow, suggesting that turbulence is a controlling factor for floc size.

[34] **Acknowledgments.** The authors thank Grace Cartwright, Todd Nelson, Bob Gammisch, Frank Farmer, Sam Wilson, Wayne Reisner, and Don Wright for their assistance with the preparation, deployment, and retrieval of the instrumentation used in this experiment. Willy Reay kindly provided the YSI 6000 s used in the experiment. This manuscript benefited from the helpful comments of two anonymous reviewers. Support for this research at VIMS was provided by the National Science Foundation Division of Ocean Sciences grants OCE-9984941 and OCE-0536572. This is contribution 2813 of the Virginia Institute of Marine Science, College of William and Mary.

References

Berhane, I., R. W. Sternberg, G. C. Kineke, T. G. Milligan, and K. Kranck (1997), The variability of suspended aggregates on the Amazon continental shelf, *Cont. Shelf Res.*, *17*, 267–285.

Deines, K. L. (1999), Backscatter estimation using broadband acoustic Doppler current profilers, paper presented at Oceans '99, Mar. Technol. Soc., Seattle, Wash.

Eisma, D. (1986), Flocculation and deflocculation of suspended matter in estuaries, *Neth. J. Sea Res.*, *20*, 183–199.

Fugate, D. C., and C. T. Friedrichs (2002), Determining concentration and fall velocity of estuarine particle populations using ADV, OBS and LISST, *Cont. Shelf Res.*, *22*, 1867–1886.

Geyer, W. R. (1993), The importance of suppression of turbulence by stratification on the estuarine turbidity maximum, *Estuaries*, *16*, 113–125.

Geyer, W. R., R. P. Signell, and G. C. Kineke (1998), Lateral trapping of sediment in a partially mixed estuary, in *Physics of Estuaries and Coastal Seas: Proceedings of the 8th International Biennial Conference on Physics of Estuaries and Coastal Seas*, edited by J. Dronkers and M. Scheffers, pp. 115–124, A. A. Balkema, Brookfield, Vt.

Geyer, W. R., J. H. Trowbridge, and M. M. Bowen (2000), The dynamics of a partially-mixed estuary, *J. Phys. Oceanogr.*, *30*, 2035–2048.

Geyer, W. R., J. D. Woodruff, and P. Traykovski (2001), Sediment transport and trapping in the Hudson River Estuary, *Estuaries*, *24*, 670–679.

Holdaway, G. P., P. D. Thorne, D. Flatt, S. E. Jones, and D. Prandle (1999), Comparison between ADCP and transmissometer measurements of suspended sediment concentration, *Cont. Shelf Res.*, *19*, 421–441.

Jackson, G. A. (1995), Comparing observed changes in particle size spectra with those predicted using coagulation theory, *Deep Sea Res., Part II*, *42*, 159–184.

Jay, D. A., and J. D. Musiak (1994), Particle trapping in estuarine tidal flows, *J. Geophys. Res.*, *99*, 20,445–20,461.

Kranck, K. (1981), Particulate matter grain-size characteristics and flocculation in a partially mixed estuary, *Sedimentology*, *28*, 107–114.

Kranck, K., and T. G. Milligan (1992), Characteristics of suspended particles at an 11-hour Anchor Station in San Francisco Bay, California, *J. Geophys. Res.*, *97*, 11,373–11,382.

Lin, J., and A. Y. Kuo (2001), Secondary turbidity maximum in a partially mixed microtidal estuary, *Estuaries*, *24*, 707–720.

McCave, I. N. (1985), Mechanics of deposition of fine-grained sediments from nepheloid layers, *Geo Mar. Lett.*, *4*, 243–245.

Postma, H. (1967), Sediment transport and sedimentation in the estuarine environment, in *Estuaries*, *Publ. 83*, edited by G. H. Lauff, pp. 158–179, Am. Assoc. for the Adv. of Sci., Washington, D. C.

Rippeth, T. P., N. R. Fisher, and J. H. Simpson (2001), The cycle of turbulent dissipation in the presence of tidal straining, *J. Phys. Oceanogr.*, *31*, 2458–2471.

Schubel, J. R. (1968), Turbidity maximum of the northern Chesapeake Bay, *Science*, *6*, 1012–1015.

Scully, M. E., and C. T. Friedrichs (2003), The influence of asymmetries in overlying stratification on near-bed turbulence and sediment suspension in a partially-mixed estuary, *Ocean Dyn.*, *53*, 208–218.

Scully, M. E., and C. T. Friedrichs (2007), The importance of tidal and lateral asymmetries in stratification to residual circulation in partially-mixed estuaries, *J. Phys. Oceanogr.*, *37*, 1496–1511.

Simpson, J. H., J. Brown, J. Matthews, and G. Allen (1990), Tidal straining, density currents, and stirring in the control of estuarine stratification, *Estuaries*, *13*, 125–132.

Smith, J. D., and S. R. McLean (1977), Spatially averaged flow over a wavy surface, *J. Geophys. Res.*, *82*, 1735–1746.

Stacey, M. T., S. G. Monismith, and J. R. Burau (1999), Observations of turbulence in a partially stratified estuary, *J. Phys. Oceanogr.*, *29*, 1950–1970.

Sternberg, R. W., I. Berhane, and A. S. Ogston (1999), Measurement of size and settling velocity of suspended aggregates on the northern California continental shelf, *Mar. Geol.*, *154*, 43–53.

Thorne, P. D., and D. M. Hanes (2002), A review of acoustic measurement for small-scale sediment processes, *Cont. Shelf Res.*, *22*, 602–632.

Traykovski, P., R. Geyer, and C. Sommerfield (2004), Rapid sediment deposition and fine-scale strata formation in the Hudson estuary, *J. Geophys. Res.*, *109*, F02004, doi:10.1029/2003JF000096.

van Leussen, W. (1988), Aggregation of particles, settling velocity of mud flocs: A review, in *Physical Processes in Estuaries*, edited by J. Dronkers and W. van Leussen, pp. 347–403, Springer, New York.

Woodruff, J. D., W. R. Geyer, C. K. Sommerfield, and N. W. Driscoll (2001), Seasonal variation of sediment deposition in the Hudson River estuary, *Mar. Geol.*, *179*, 105–119.

C. T. Friedrichs, Virginia Institute of Marine Science, P. O. Box 1346, Gloucester Point, VA 23062, USA.

M. E. Scully, Woods Hole Oceanographic Institution, Applied Ocean Physics and Engineering, Mail Stop 10, Woods Hole, MA 02543, USA. (mscully@whoi.edu)